Contrib. Astron. Obs. Skalnaté Pleso **34**, 167 – 196, (2004)

A description of the SHELLSPEC code

J. Budaj[1,2] **and M.T. Richards**[1]

[1] *Dept. of Astronomy and Astrophysics, Penn State University, Davey Lab. 525, University Park, PA 16802, USA*

[2] *Astronomical Institute of the Slovak Academy of Sciences 059 60 Tatranská Lomnica, The Slovak Republic, (E-mail: budaj@astro.psu.edu)*

Received: January 30, 2004; Accepted: August 16, 2004

Abstract. Program SHELLSPEC is designed to solve simple radiative transfer along the line of sight in moving media. The scattered light from a central object can be taken into account assuming an optically thin environment. Output intensities are then integrated through the 2D projection surface of a 3D object. The assumptions include LTE and optional known state quantities and velocity fields in 3D. Optional (non)transparent objects such as a spot, disc, stream, jet, shell or stars as well as an empty space may be defined (embedded) in 3D and their composite synthetic spectrum calculated. The stars may have the Roche geometry and known intrinsic spectra. Synthetic light curves or trailing spectrograms can be produced by changing your view points on the 3D object.

An application to the accretion disc system of TT Hya type (Algol-type eclipsing binary with a disc) is included and the influence of various effects on the emerging spectrum is studied.

Key words: Radiative transfer – Accretion, accretion discs – Stars: binaries: close – Stars: binaries: eclipsing – Stars: novae, cataclysmic variables

1. Introduction

There are sophisticated computer codes for calculating and inverting light curves or spectra of binary stars with various shapes or geometry including the Roche model (Lucy 1968; Wilson & Devinney 1971; Mochnacki & Doughty 1972; Rucinski 1973; Hill 1979; Zhang et al. 1986; Djurasevic 1992; Drechsel et al. 1994; Vinkó et al. 1996; Hadrava 1997; Bradstreet & Steelman 2002; Pribulla 2004). In these codes, the stars are assumed to be nontransparent, stripped of any circumstellar matter and their main concern or purpose is to deal with the complicated geometry. However, it is often the case that such nontransparent objects are embedded in some moving optically thin environment (Cherepashchuk et al. 1984) and/or are accompanied by shells, discs, jets or streams and one would need to know at least an approximate spectrum, light curve and trailing spectrogram. Often the 3D model (behavior of state quantities and velocity field) is known or expected as a result of hydrodynamic simulations or observational

constraints (see for example Richards & Ratliff 1998). Unfortunately, 3D NLTE calculations including complex hydrodynamics are difficult to carry out so one alternative has been to perform a simple volume integration of emissivity, which is often too oversimplified for the particular problem.

On the other hand, highly sophisticated model atmospheres and spectrum synthesis codes were developed assuming NLTE and plane-parallel atmospheres of hot stars (Hubeny 1988; Hubeny & Lanz 1992, 1995; Hubeny et al. 1994), spherically symmetric atmospheres (Kubát 2001), or stellar winds (Krtička & Kubát 2002). There are also sophisticated stationary plane-parallel line-blanketed model atmospheres and spectrum synthesis codes for a large variety of stars assuming LTE (Kurucz 1993a, 1993b; Smith & Dworetsky 1988 and many others). However, these are very specialized codes and their main concern and purpose is to calculate the spectrum emerging from a stellar atmosphere and it is difficult to apply them to the various cases outlined above. An exception is the special case of circumstellar matter in the form of accretion discs in CV's. In this case, the disc is either approximated by a set of geometrically thin but optically thick static local atmospheres and the output radiation is a sum of properly Doppler shifted local emerging intensities (Orosz & Wade 2003; Wade & Hubeny 1998; la Dous 1989) or, in case of optically thin discs or accretion disc winds, the Sobolev approximation is used (Proga et al. 2002; Long & Knigge 2002; Rybicki & Hummer 1983). Horne & Marsh (1986) solved the radiative transfer along the line of sight in a moving thin disc assuming liner shear and showed that it is often important.

The aim of this paper is not to compete with the codes and models mentioned above but rather to bridge the gap in these present approaches and provide a tool which would solve in LTE the simple radiative transfer along the line of sight in an optional optically thin 3D moving medium with the possible nontransparent objects embedded in. We present the new code to synthesize the composite spectrum of accretion structures in close binaries which undergo direct impact accretion, as in the close Algols. However, the code is quite a multi-purpose, independent, and flexible tool which can also calculate a light curve or a trailing spectrogram where necessary, or can be used to study various objects or effects.

2. Basic astrophysics

2.1. Radiative transfer

In the following analysis, the calculations are carried out in the observer's Cartesian frame with z pointing towards the observer. The radiative transfer equation along the line of sight is:

$$dI_\nu = (\epsilon_\nu - \chi_\nu I_\nu)dz \tag{1}$$

where I_ν is the specific monochromatic intensity at the frequency ν, χ_ν is the opacity, ϵ_ν is the emissivity and z is the distance along the beam. It is conve-

nient to split the opacity into two contributions, the true absorption κ_ν and the scattering σ_ν:

$$\chi_\nu = \kappa_\nu + \sigma_\nu. \tag{2}$$

Assuming LTE, the line opacity corrected for a stimulated emission is stated simply as:

$$\chi_\nu^{line} = (1 - e^{-\frac{h\nu}{kT}}) N_l B_{lu} h\nu \varphi_{lu}(\nu - \nu_0)(4\pi)^{-1} \tag{3}$$

where h is the Planck constant, $h\nu$ is the energy of the transition from the lower level l to the upper level u, k is the Boltzmann constant, T is the temperature, N_l is the population of the l-th state of the corresponding ion, and B_{lu} is the Einstein coefficient for the whole solid angle. The velocity field enters the equation via the shifted normalized Voigt profile $\varphi_{lu}(\nu - \nu_0)$ where

$$\nu_0 = \nu_{lu} \left(\frac{v_z(z)}{c} + 1 \right) \tag{4}$$

where ν_{lu} is the laboratory frequency of the line and $v_z = \boldsymbol{v}.\boldsymbol{n}$ is the radial velocity (positive towards the observer) or projection of the local velocity vector $\boldsymbol{v}$ to the line of sight unit vector $\boldsymbol{n}$. The Einstein coefficient, B_{lu}, is related to the oscillator strength, f_{lu}, by:

$$B_{lu} = \frac{4\pi^2 e^2 f_{lu}}{m_\mathrm{e} c h \nu_{lu}} \tag{5}$$

where e, m_e are the electron charge and mass, respectively and c is the speed of light. The shape of the Voigt profile is determined by the thermal and the microturbulent broadening, v_{trb}, characterized by the Doppler half-width

$$\Delta\nu_D = \frac{\nu}{c} \sqrt{\frac{2kT}{m} + v_{trb}^2} \tag{6}$$

as well as by the damping broadening characterized by the frame damping parameter

$$a = \gamma / (4\pi \Delta\nu_D) \tag{7}$$

where the damping constant

$$\gamma = \gamma_{Nat.} + \gamma_{Stark} + \gamma_{VDW} \tag{8}$$

includes the contribution from the Natural, Stark and Van der Waals broadening. In the case of LTE, all the line opacity is due to the true absorption process i.e.:

$$\kappa_\nu^{line} = \chi_\nu^{line} \tag{9}$$

We also included four other continuum opacity sources: the HI bound-free opacity, the HI free-free opacity, Thomson scattering and Rayleigh scattering on

neutral hydrogen.
For HI bound-free opacity, based on Gray (1976) and Mihalas (1978), we have:

$$\kappa_\nu^{HIbf} = \frac{2.8154 \times 10^{29}}{\nu^3} n_{HI} \frac{2}{u_{HI}} (1 - e^{-\frac{h\nu}{kT}}) \times \left[\sum_{n=n_0}^{n_0+2} (\frac{g_n^{bf}}{n^3} e^{-\frac{-\chi_n}{kT}}) + \frac{kT}{2I} (e^{-\frac{-\chi_{n_0+3}}{kT}} - e^{-\frac{-I}{kT}}) \right] \quad (10)$$

where n_{HI} is the neutral hydrogen number density, u_{HI} is its partition function, n is the main quantum number, n_0 is the value of n for the lowest level of importance (levels with $n < n_0$ have their photoionization edges at higher frequency than ν and thus do not contribute to the opacity at ν), $g_n^{bf}(\nu)$ is the bound-free Gaunt factor of the particular level, χ_n is the excitation potential of the level and I is the ionization potential of the ion. In the formula above, the contribution from the levels: $n_0, n_0 + 1, n_0 + 2$ is taken into account explicitly while the contribution of the higher levels with $n > n_0 + 2$ is integrated.
The HI free-free opacity (Mihalas 1978) is:

$$\kappa_\nu^{HIff} = 3.69 \times 10^8 g^{ff} \frac{n_e n_{HII}}{\nu^3 T^{1/2}} (1 - e^{-\frac{h\nu}{kT}}) \quad (11)$$

where $g^{ff}(T, \nu)$ is the free-free Gaunt factor, n_e is the electron number density and n_{HII} is the proton number density.
Thomson scattering opacity (Mihalas 1978) is:

$$\sigma_\nu^{TS} = n_e \sigma_e = 6.65 \times 10^{-25} n_e \quad . \quad (12)$$

For Rayleigh scattering on neutral hydrogen we adopted the following expression from Kurucz (1970):

$$\sigma_\nu^{RS} = n_{HI,0} [5.799\, 10^{-13} + (1.422\, 10^{-6} + 2.784w)w] w^2 \quad (13)$$

where $w = 10^{-16} [min(\nu, 2.463\, 10^{15})/c]^2$ and $n_{HI,0}$ is the population of the ground state of neutral hydrogen.
The total true absorption κ_ν is the sum of the three opacity sources:

$$\kappa_\nu = \kappa_\nu^{line} + \kappa_\nu^{HIbf} + \kappa_\nu^{HIff}. \quad (14)$$

The total scattering σ_ν is:

$$\sigma_\nu = \sigma_\nu^{TS} + \sigma_\nu^{RS}. \quad (15)$$

The thermal emissivity associated with the true absorption can then be written as

$$\epsilon_\nu^{th} = B_\nu(T(z)) \kappa_\nu \quad (16)$$

where B_ν is the Planck function for the local value of the temperature. For scattering emissivity we have

$$\epsilon_\nu^{sc} = \iint \sigma(\nu', \nu, \boldsymbol{n'}, \boldsymbol{n}) I(\nu', \boldsymbol{n'}) d\nu' \frac{d\omega'}{4\pi} \quad (17)$$

where $\sigma(\nu', \nu, \boldsymbol{n'}, \boldsymbol{n})$ is the scattering coefficient containing the general redistribution function. It is this term which causes the main difficulty, since apart from redistributing the frequencies ($\nu' \rightarrow \nu$), it also couples the radiation in one direction $\boldsymbol{n}$ with the radiation field in all other directions $\boldsymbol{n'}$. However, in many applications (e.g., optically thin shells) this term can either be neglected or governed by the scattering of light from the central object. We assume coherent isotropic scattering (as seen from the scattering particle frame) from a blackbody or from a central spherical star with precalculated surface intensity $I_\nu^\star$ or flux $F_\nu^\star$. In this case the emissivity reduces to:

$$\epsilon_\nu^{sc} = \sigma_\nu J_\nu \tag{18}$$

where J_ν is the mean intensity. Ignoring limb darkening, J_ν can be approximated by:

$$J_\nu \approx I_{\nu_1}^\star \omega / 4\pi \tag{19}$$

where ω is the solid angle subtended by the central star and

$$\omega/4\pi = \frac{1}{2}\left(1 - \sqrt{1 - \left(\frac{R_\star}{r}\right)^2}\right) \tag{20}$$

where $R_\star$ is the radius of the central star and r is the distance from the center (of the star/grid) and

$$\nu_1 = -\nu\left(\frac{v_1}{c} - 1\right) \tag{21}$$

and

$$v_1 = -\frac{\boldsymbol{r}.(\boldsymbol{v} - \boldsymbol{v}_\star)}{r} + v_z \tag{22}$$

where $\boldsymbol{v}$ is the velocity field vector at the given point specified by the vector $\boldsymbol{r}$ and $\boldsymbol{v}_\star$ is the velocity of the center of mass of the central object.
For $R_\star/r << 1$ an approximation including the limb darkening and the non-isotropic dipole phase function $g(\boldsymbol{n'}, \boldsymbol{n}) = \frac{3}{4}(1 + (\boldsymbol{n'}.\boldsymbol{n})^2)$ could be used:

$$\epsilon_\nu^{sc} = \frac{3}{4}\left(1 + \frac{r_z^2}{r^2}\right)\sigma_\nu J_\nu \tag{23}$$

where

$$J_\nu \approx \frac{F_{\nu_1}^\star}{4\pi}\frac{R_\star^2}{r^2} \tag{24}$$

where

$$F_{\nu_1}^\star = \pi I_{\nu_1}^\star\left(1 - \frac{u}{3}\right) \tag{25}$$

where u is the limb darkening coefficient.
The total emissivity is then

$$\epsilon_\nu = \epsilon_\nu^{th} + \epsilon_\nu^{sc} \tag{26}$$

and the total source function is:

$$S_\nu = \epsilon_\nu / \chi_\nu. \tag{27}$$

The flux, F_ν, from the object at the Earth is then obtained by the integration of the output intensities I_ν^{out} through the 2D projection surface of the 3D object:

$$F_\nu = \int I_\nu^{out} d\Omega \tag{28}$$

where Ω is the solid angle on the sky subtended by the shell and

$$F_\nu = \iint \frac{I_\nu^{out}}{D^2} dx dy \tag{29}$$

where D is the distance to the shell from the Earth.

2.2. Roche geometry

Both objects, star and companion, may have shapes according to the Roche model for detached or contact systems. Descriptions of the Roche model can be found in Kopal (1959), Plavec & Kratochvil (1964), Mochnacki & Doughty (1972), Hilditch (2001) and many other papers and books. Let us assume a Cartesian coordinate system (x,y,z) centered on one of the stars (labeled as 1) such that the companion (labeled as 2) is at (1,0,0) and revolves around the z axis in the direction of positive y axis. Let the mass ratio, q, always be m_2/m_1 or 'companion/star' and $q < 1$ will indicate the companion is lighter while $q > 1$ means the central star is lighter. Then, the normalized Roche potential, C, is expressed as:

$$C(x,y,z) = \frac{2}{(1+q)r_1} + \frac{2q}{(1+q)r_2} + \left(x - \frac{q}{1+q}\right)^2 + y^2 \tag{30}$$

where $r_1 = \sqrt{x^2+y^2+z^2}$ and $r_2 = \sqrt{(x-1)^2+y^2+z^2}$. The Roche surface of a detached component is defined as an equipotential surface $C_s = C(x_s, y_s, z_s)$ passing through the substellar point (x_s, y_s, z_s) (point on the surface of the star in between the stars, $0 < x_s < 1, y_s = z_s = 0$) which is localized by the 'fill-in' parameter $f_i \leq 1$. We define this by:

$$f_i = x_s / L_{1x}, \qquad f_i = (1 - x_s)/(1 - L_{1x}) \tag{31}$$

for the primary and the secondary, respectively. L_{1x} is the x coordinate of the L1 point L1$(L_{1x}, 0, 0)$. The Roche equipotential surface C_s of a contact system will be defined by the fill-out parameter $1 < f_o \leq 2$:

$$f_o = \frac{C1 - C_s}{C1 - C2} + 1 \tag{32}$$

where potentials $C1, C2$ correspond to the potentials at the L1 and L2 points, respectively. First, we calculate L1, L2, C_s and x-boundaries of the object using the Newton-Raphson iteration method e.g.,

$$x_{i+1} = x_i - \frac{C(x_i, 0, 0) - C_s}{C_x(x_i, 0, 0)} \tag{33}$$

and then the 3D shape of the surface is solved using the Newton-Raphson iteration in y and z coordinates with the precision of about 10^{-5}. Here are the derivatives necessary for the task:

$$C_x = \frac{\partial C}{\partial x} = -\frac{2x}{(1+q)r_1^3} - \frac{2q(x-1)}{(1+q)r_2^3} + 2x - \frac{2q}{1+q} \tag{34}$$

$$C_y = \frac{\partial C}{\partial y} = -\frac{2y}{(1+q)r_1^3} - \frac{2qy}{(1+q)r_2^3} + 2y \tag{35}$$

$$C_z = \frac{\partial C}{\partial z} = -\frac{2z}{(1+q)r_1^3} - \frac{2qz}{(1+q)r_2^3} \tag{36}$$

$$\frac{\partial^2 C}{\partial x^2} = \frac{6x^2}{(1+q)r_1^5} + \frac{6q(x-1)^2}{(1+q)r_2^5} - \frac{2}{(1+q)r_1^3} - \frac{2q}{(1+q)r_2^3} + 2 \tag{37}$$

Gravity darkening is taken into account by varying the surface temperature according to the following law:

$$T/T_p = (g/g_p)^\beta \tag{38}$$

where g is the normalized surface gravity, β is the gravity darkening coefficient, T_p, g_p are the temperature and gravity at the rotation pole. The normalized gravity vector is $\boldsymbol{g} = (C_x, C_y, C_z)$ and:

$$g = \sqrt{C_x^2 + C_y^2 + C_z^2}. \tag{39}$$

The gravity darkening factor of the surface intensity is then calculated as:

$$f_{GD} = B_\nu(T)/B_\nu(T_p). \tag{40}$$

Limb darkening is taken into account using Eq.49 and by calculating the cosine of the angle θ between the line of sight unit vector $\boldsymbol{n} = (n_x, n_y, n_z)$ and a normal to the surface:

$$\cos\theta = -\boldsymbol{n}.\boldsymbol{g}/g = -\frac{n_x C_x + n_y C_y + n_z C_z}{\sqrt{C_x^2 + C_y^2 + C_z^2}}. \tag{41}$$

Reflection effect is not included in the present version.

3. Numerical performance

3.1. Solution of the radiative transfer equation

A number of optional objects (transparent, nontransparent, empty space, ...) can be defined within the model and the line of sight may cross more of them within a few grid points. A simple and stable method is needed to cope with such velocity, density, temperature fields which are optional and are allowed to be noncontinuous. Our problem is that of the integration of a first order ordinary differential equation with known initial values at one boundary. The equation of the radiative transfer along the line of sight at the frequency ν can be written in the discretised form:

$$\frac{I_{i+1} - I_i}{z_{i+1} - z_i} = \epsilon_{i+1/2} - \chi_{i+1/2}(I_{i+1} + I_i)/2 \tag{42}$$

and simply integrated via the following recurrent formula:

$$I_{i+1} = \frac{S_{i+1/2}}{A + 1/2} + I_i \frac{A - 1/2}{A + 1/2} \tag{43}$$

where

$$A = \frac{1}{\chi_{i+1/2}(z_{i+1} - z_i)} \tag{44}$$

and

$$S_{i+1/2} = \frac{\epsilon_{i+1/2}}{\chi_{i+1/2}}, \quad I_1 = 0 \tag{45}$$

where

$$\epsilon_{i+1/2} = \frac{\epsilon_i + \epsilon_{i+1}}{2} \quad , \quad \chi_{i+1/2} = \frac{\chi_i + \chi_{i+1}}{2}. \tag{46}$$

If the line of sight happens to hit a nontransparent object, the object is skipped and the integration starts on the other side of the object with the boundary condition:

$$I_1 = I^\star(\nu_2) f_{LD} f_{GD} \quad \text{or} \quad I_1 = B_{\nu_2}(T_{eff}) f_{LD} f_{GD} \tag{47}$$

where

$$\nu_2 = -\nu \left(\frac{v_z^\star}{c} - 1 \right) \tag{48}$$

and $v_z^\star$ is the radial velocity of the surface of the nontransparent object where it intersects the line of sight. Rotation of the nontransparent objects is fully taken into account here by including it into the calculations of $v_z^\star$. f_{LD} is a limb darkening factor:

$$f_{LD} = 1 - u + u \cos\theta \tag{49}$$

where u is the limb darkening coefficient and θ is the angle between the normal to the surface of the nontransparent object and the line of sight. f_{GD} is a gravity

darkening factor which is important in the case of Roche geometry (see Sec.2.2) and in which case $T_{eff} = T_p$ is the temperature at the rotation pole of a detached star or the temperature at the rotation pole of the more massive star in the case of a contact system, otherwise, it is the common effective temperature of the spherical star. If the line of sight happens to pass through an empty space this region is also skipped and the integration continues with $I_{i+1} = I_i$.

3.2. Rotation of the observer's frame

The SHELLSPEC code enables the user to look on the object from different points of view and to calculate the corresponding spectra. The input model of the shell is defined in its 'body frozen' Cartesian coordinates (x'', y'', z'') with the z'' axis corresponding to the intrinsic rotation axis of the model. The spectrum is always calculated in the observer's 'line of sight' Cartesian frame (x, y, z) with z pointing to the observer and which has the same center of coordinates (see Figure 1.). We first calculate the body frozen coordinates corresponding to the grid points of the line of sight mesh by rotating the latter along the x axis by an angle i (the inclination of the intrinsic rotation axis of the model to the line of sight) to get new subordinate prime coordinates (x', y', z') and then by rotating the prime coordinates by a sequence of angles α around the $z'' = z'$ axis:

$$\begin{aligned} x' &= x & \qquad z'' &= z' \\ y' &= y\cos i - z\sin i & \qquad x'' &= x'\cos\alpha + y'\sin\alpha \\ z' &= z\cos i + y\sin i & \qquad y'' &= y'\cos\alpha - x'\sin\alpha \end{aligned} \tag{50}$$

Then we interpolate all the scalar and vector quantities from the body frozen coordinates to the grid points of the rotated observer's frame and, finally, make a back-transformation of the vector quantities (velocity field) as listed below:

$$\begin{aligned} f(x'', y'', z'') = {} & (1-t)(1-u)(1-v)f_{i,j,k} + t(1-u)(1-v)f_{i+1,j,k} \\ & + tu(1-v)f_{i+1,j+1,k} + (1-t)u(1-v)f_{i,j+1,k} \\ & + (1-t)(1-u)vf_{i,j,k+1} + t(1-u)vf_{i+1,j,k+1} \\ & + tuvf_{i+1,j+1,k+1} + (1-t)uvf_{i,j+1,k+1} \end{aligned} \tag{51}$$

where

$$\begin{aligned} t &= (x'' - x''_i)/(x''_{i+1} - x''_i) \\ u &= (y'' - y''_j)/(y''_{j+1} - y''_j) \\ v &= (z'' - z''_k)/(z''_{k+1} - z''_k) \end{aligned} \tag{52}$$

Back-transform of vector quantities:

$$\begin{aligned} v'_z &= v''_z & \qquad v_x &= v'_x \\ v'_x &= v''_x\cos\alpha - v''_y\sin\alpha & \qquad v_y &= v'_y\cos i + v'_z\sin i \\ v'_y &= v''_y\cos\alpha + v''_x\sin\alpha & \qquad v_z &= v'_z\cos i - v'_y\sin i \end{aligned} \tag{53}$$

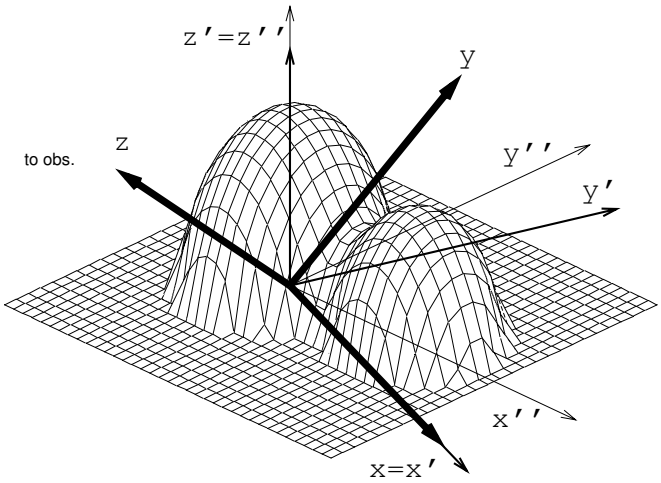

Figure 1. Definition of the 'body frozen' frame (x'', y'', z'') with the z'' axis corresponding to the intrinsic rotation axis of the model and the 'line of sight' frame (x, y, z) with z pointing to the observer.

3.3. Level populations and miscellaneous notes

The code assumes the known behavior of state quantities: temperature T, density ρ, and electron number density n_e. The atomic number density of all atoms is calculated as:

$$n_a = \frac{\rho}{wm} = \rho \frac{\sum a_i}{\sum a_i m_i} \tag{54}$$

where wm is the mean molecular weight and a_i, m_i are the element abundances and atomic masses respectively. Abundances are defined relative to hydrogen:

$$a_i = n_i / n_H \tag{55}$$

where n_i, n_H are the element and hydrogen number densities. The hydrogen abundance relative to the total atomic number density is $a'_H = 1/\sum a_i$. Once n_a is known hydrogen number density is calculated as $n_H = a'_H n_a$ and element number densities then follow from their abundances. Solar abundances are assumed (Grevesse & Sauval 1998) but the user is allowed to change all the element abundances. The level populations are obtained from the Boltzmann and Saha equations. Partition functions were taken from the UCLSYN code (Smith & Dworetsky 1988, Smith 1992). A FORTRAN77 code containing the partition

function routines is also available in Budaj, Dworetsky & Smalley (2002). The Gaunt factors are calculated with the subroutines taken from the SYNSPEC code (Hubeny et al. 1994). Damping constants can be found from the VALD atomic line database (Kupka et al. 1999) or in Kurucz (1993a). If the damping constants are not known they are estimated in the code in the way analogous to the SYNSPEC code:

$$\begin{aligned} \gamma_{Nat.} &= 2.4734\,10^{-22}\nu_{lu}^2 \\ \gamma_{Stark} &= 10^{-8} n_e n_{eff}^5 \\ \gamma_{VDW} &= 4.5\,10^{-9} X^{0.4} (n_{HI} + 0.42 n_{HeI}) \left(\tfrac{T}{10^4}\right)^{0.3} \end{aligned} \tag{56}$$

where n_{HeI} is the neutral helium number density and the reader is referred to the SYNSPEC source code for the details on X, n_{eff}. CGS units are used within the code and the manuscript if not specified otherwise. The user needs to ensure that the model is consistent with the abundances and is realistic, e.g., that it satisfies the continuity equation and other conditions where necessary. The user can easily modify the subroutine SMOD1 and insert his/her own prescription for a model there or load a precalculated model from a file.

3.4. Adopted routines

Several routines used in this code were adopted from other sources. These are:
pfdwor (from UCLSYN, Smith & Dworetsky 1988);
voigt0, state0, gaunt, gfree (from SYNSPEC, Hubeny et al. 1994); and
locate, hunt (from Numerical Recipes, Press et al. 1986).
We also used a few sections from our previous original codes for calculations of radiative accelerations in stellar atmospheres of hot stars (Budaj & Dworetsky 2002). Apart from the above, the code was written from scratch and provides a quite independent tool to study a large variety of objects and effects. Although a substantial effort was devoted to check the calculations there is no guarantee that the code is error free and we would appreciate any bug/error reports.

4. Compilation

The code is distributed in the form of several files:

shellspecxx.f	the source code
pfdwor.inc	an include file with the partition functions subroutine
param.inc	an include file with array dimensions
shellspec.in	an example of the main input file
line.dat	an example of the line data input file
shellspec.mod	an example of the input 3D model of the shell
abundances	an example of the abundances input file
starspec1	an example of the input spectrum of the primary star

starspec2 an example of the input spectrum of the secondary star
starspec3 an example of the input spectrum of the 'third body'.

The code is written in standard FORTRAN77 which makes it highly portable. To compile and link the code under LINUX use the following command:

g77 shellspecxx.f -o shellspec

where 'xx' stands for the current version of the code. To run the code write:

./shellspec

You may need to adjust the array dimensions according to the available memory. As needed, modify the array dimensions in the file param.inc. The most memory consuming parameters are: $ndim1, ndim2, ndim3$ which specify the xyz dimensions and possibly also $mfreq$ which determines the number of frequency points.

5. Input

The list of all possible input files with their associated unit numbers follows. These input files are described in more detail in the subsections below:

shellspec.in -(9) main input (geometry, objects...)
line.dat - (8) atomic data for the spectral line
shellspec.mod - (10) input 3D model of the shell (optional if $imodel = 2$)
abundances - (7) abundances (optional if $ichemc = 1$)
starspec1 - (12) spectrum of the primary star (optional if $lunt1 > 0$)
starspec2 - (13) spectrum of the secondary (optional if $lunt2 > 0$)
starspec3 - (14) spectrum of the 'third body' (optional if $lunt3 > 0$)

5.1. shellspec.in

This is the main input file where you can describe the geometry, dynamics and optical properties of the moving medium which we often refer to as a shell or a model. However, it can consist of many objects of various types (unfortunately, one of them is also called a shell but the difference should be obvious from the context). Various numerical and technical details are also specified in this file.

Imagine this shell as frozen in one instant of time, overlay it with the Cartesian coordinates (x'', y'', z'') as seen in Figure 1 so that you have a convenient object, e.g., a hot star in the center and z'' corresponds to the intrinsic axis of revolution of the shell and describe its properties (state quantities and velocity field) using these coordinates in this file. You can also load a precalculated

model from an extra file. Various transparent and nontransparent objects can be defined here. These include:

- STAR: a central nontransparent object which can rotate as a solid body with an optional inclination of the rotational axis and have a net space velocity. Can be treated as a blackbody or have its own spectrum. Limb darkening can be applied to it. Also, the scattered light from this object can be taken into account neglecting its rotation. Can be surrounded by a Keplerian disc which is specified separately. May be of the spherical or Roche shape. Designed to model mainly hotter or more luminous stellar components.

- COMPANION: a nontransparent object which can rotate as a solid body with an optional inclination of the rotational axis and have a net space velocity. Limb darkening can be applied to it. Can be treated as a black body or have its own spectrum. May be of the spherical or Roche shape. Designed to model mainly a secondary (cooler or fainter component of a binary system).

- SPOT: a spherical object which can rotate as a solid body with an optional inclination of the rotational axis and have a net space velocity. Designed to model mainly spots on accretion discs, direct impact regions, rotating circum-stellar (circum-binary) shells or third bodies.

- DISC: has either the shape of a rotating wedge (space complement to two opposite cones) or of a slab surrounding the central object. It is farther constrained by two spherical surfaces: its inner and outer radius (r_{in}, r_{out}). This structure can be inclined if necessary. The velocity field $\boldsymbol{v}$ of the disc adopted depends on $M_\star$, the mass of the central object and is Keplerian within the disc plane, namely:

$$\omega(r) = \sqrt{G\frac{M_\star}{r^3}} \qquad\qquad \boldsymbol{v} = \boldsymbol{\omega} \times \boldsymbol{r} \tag{57}$$

  where G is the gravitational constant, $\boldsymbol{\omega}, \boldsymbol{r}$ are the angular velocity and radius vectors, respectively. It is possible to vary the densities as a power law: $\rho(r) = \rho(r_{in})(r/r_{in})^{edendc}$, $\quad n_e = n_e(r_{in})(r/r_{in})^{edendc}$ or adopt the following temperature stratification if necessary:

$$T(r) = T_{dc}\left(\frac{R_\star}{r}\right)^{\frac{3}{4}}\left(1 - \sqrt{\frac{R_\star}{r}}\right)^{\frac{1}{4}}. \tag{58}$$

  Here, T_{dc} is the characteristic temperature (Pringle 1981). Note that maximum disc temperature in this representation is about $0.488T_{dc}$. Designed to model mainly accretion discs.

- STREAM: has the shape of a cylinder with uniform velocity. Designed to model mass transfer streams.

– JET: has the shape of one or two opposite cones emerging from the center. It allows optional inclination and is farther limited by its inner and outer radius. Designed to model mainly jets or, e.g., 'shadows' cast by a cool, extended secondary from a more compact hot primary.

– SHELL: has the shape of a shell surrounding the central object. A few velocity fields are built in:

$$v(r) = v_{sh} \quad , \quad v(r) = v_{sh} \left(\frac{r}{r_{in}} \right)^{evelsh} \quad , \quad v(r) = v_{sh} \left(1 - \frac{r_c}{r} \right)^{evelsh} \tag{59}$$

while the temperature is kept fixed and densities are either constant or satisfy the continuity equation (see 'shellspec.in' for more information).

– BACKGROUND: is designed to add more flexibility to the code and to fill the region not occupied by any of the previous objects at least with a uniformly radially expanding medium when necessary. It may help to reduce a numerical noise too by the appropriate choice of state quantities.

Most of these objects can be made nontransparent blackbody, dark matter, or empty space by setting their density to unrealistic values within certain density intervals. There is also a way to ascribe an intrinsic spectrum to any of these objects using parameters $lunt1, lunt2$ and $lunt3$. The detailed description of all variables and their units is very extensive to fit into this paper and can be found attached at the end of the example 'shellspec.in' file for easy orientation.

5.2. line.dat

This file contains the atomic data for the spectral lines in the format identical to the SYNSPEC code. Each line of input corresponds to one spectral line with:

```
c       dll -wavelength [nm]
c       cod -element.ion cod, e.g. 26.02. It is interpreted as:
c         26=atomic number=iron, 02=2xtimes ionized i.e. FeIII line
c       gf -log_10 (gf)
c       elo,eup -energy of the lower and upper level in [1/cm]
c       qlo -quantum number -J of the lower level[=>stat.weight=2*J+1]
c       qup -quantum number -J of the upper level[=>stat.weight=2*J+1]
c       gr0,gs0,gw0-radiative, Stark, Van der Waals damping constants
```

5.3. shellspec.mod

The file is read if $imodel = 2$. It contains the model of the shell and is read with the following commands. Consult the example file if necessary.

```
c       nbod1,nbod2,nbod3 -number of x,y,z grid points
c       far,fat,faz -define the x,y,z grid points [cm]
c       ftemp, fpress, fdens, fne -temperature,pressure, density,
c               electron number density, respectively [cgs]
c       fvr,fvt,fvz,fvtrb -x,y,z components of the velocity field [cm/s]
c       fvtrb -turbulence [cm/s]
        read(10,*)nbod1,nbod2,nbod3
```

```
        read(10,*)(far(i),i=1,nbod1)
        read(10,*)(fat(i),i=1,nbod2)
        read(10,*)(faz(i),i=1,nbod3)
        do 30 i=1,nbod1
        do 20 j=1,nbod2
        do 10 k=1,nbod3
          read(10,*)ftemp(i,j,k),fpress(i,j,k),fdens(i,j,k),fne(i,j,k)
     p    ,fvr(i,j,k),fvt(i,j,k),fvz(i,j,k),fvtrb(i,j,k)
10      continue
20      continue
30      continue
```

5.4. abundances

The file is read if $ichemc = 1$, otherwise built in solar abundances are assumed. The number of abundances (input lines) is read from the first line ($nichem$). $nichem$ lines follow with atomic number (ii) and abundance (abii) of the elements whose abundance you wish to change. Abundance is the element number density relative to hydrogen. Consult the example file if necessary.

5.5. starspec1

Intrinsic, not rotationally broadened spectrum of the central star (1. density interval). If $lunt1 > 0$, two columns are read: xstar1, star1, where xstar1 is wavelength in Å and star1 is either Eddington flux H_λ in [erg/cm^2/s/Å] i.e. the same as output of SYNSPEC ($lunt1 = 1$) or central intensity I_ν in [erg/cm^2/s/Hz/sterad] ($lunt1 = 2$). If your data are not in the units required you can use $xunt1, yunt1$ parameters to convert otherwise set $xunt1 = yunt1 = 1.0$.

5.6. starspec2, starspec3

The same input as in starspec1 except that the relevant quantities are named $lunt2, xunt2, yunt2$ or $lunt3, xunt3, yunt3$ in starspec2 and starspec3, respectively, corresponding to 2. and 3. density intervals.

6. Output

Here is a list of all output files with their unit numbers.

shellspec.out - (2) more detailed output
fort.xx - (21,21+iang) 2D images at some frequency
shellspectrum - (4) spectrum of the shell
lightcurve - (11) light curve or trailed spectrogram

6.1. shellspectrum

The file contains several blocks separated by a blank line. Each block corresponds to one rotation, the view point on the shell. The block has 6 columns:

(1) lambda [Å], (2) velocity corresponding to lambda ($c\Delta\lambda/\lambda_{lu}$) [$km\,s^{-1}$], (3) F_ν, absolute flux at the Earth [$erg/cm^2/s/Hz$], (4) F_λ, absolute flux at the Earth [$erg/cm^2/s/cm$], (5) normalized flux, (6) normalized flux shifted in y-axis for each subsequent rotation by the value 'offset' for easy plotting.

6.2. lightcurve

This file contains several blocks separated by a blank line. Each block corresponds to one rotation, the phase of the shell. The block has 4 columns: (1) phase, (2) radial velocity [$km\,s^{-1}$], (3) magnitude $= -2.5\log_{10} F_\lambda$, and (4) normalized flux.

6.3. shellspec.out

This file contains more detailed output of various quantities (opacities, emissivities, optical depth, ...), mainly details along one particular ray (line of sight) and frequency specified in the input by 'ionu, ior, iot'.

6.4. fort.xx

Here, fort.xx corresponds to fort.21 and higher. These are 2D-xy projection images of the shell at different phases at the frequency specified by *ionu*. Each file corresponds to one phase. Each file consists of several blocks separated by a blank line. Each block corresponds to one x-value (y-varies) and has 3 columns: (1) x [cm], (2) y [cm], (3) I_ν in [$erg/cm^2/s/Hz/sterad$].

7. Demonstration of an artificial model

As an illustration, we include a few pictures calculated for an artificial spectral line and an artificial test model. It includes two stars, a Keplerian equatorial disc around a bigger primary, a slightly inclined jet and a slowly expanding shell surrounding the system. Stars are treated as blackbodies, the primary is a sphere with limb darkening imposed on while the secondary fills its Roche lobe and is subject to gravity darkening only. The centers of the jets and shell have no net space velocity while the net velocity of the center of the disc corresponds to that of the primary. Jets presess with the orbital period. Calculations were performed for about 50 phases as seen from the orbital plane. The model was defined in a cube with 101x101x101 points and spectrum was calculated at 241 frequency points. For the sole purpose of this illustration, the input values were manipulated so that a contribution from each object could be seen. Figure 2 shows a 2D projection image ($I_\nu^{out}(x,y)$) of a test model in the continuum (at a frequency in the far wing of the spectral line) taken roughly at quadrature. Different shapes of the primary and secondary illustrate the effects of limb darkening and gravity darkening. Figure 3 shows the overall light curve of the model

as it revolves with apparent primary and secondary minima at each frequency. Figure 4 displays the trailed spectrogram. The central emission comes from the slowly expanding shell. The double wave is caused by the two jet cones. The two single waves (blue and red) originate in the disc and reflect its orbital motion tracing that of the primary. Observe a depression in both single waves near the primary minimum caused by the eclipse of the approaching and receding part of the disc by the secondary star.

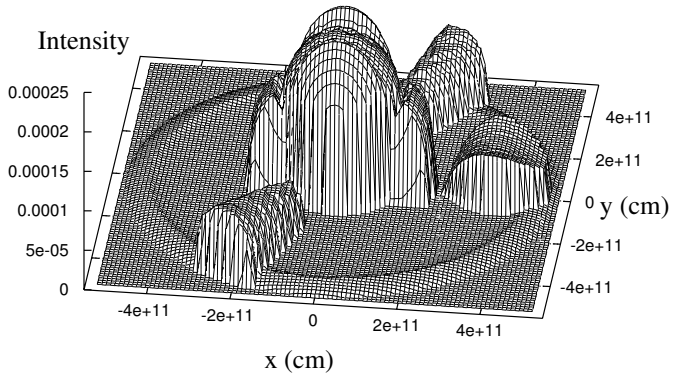

Figure 2. 2D projection image, $I_\nu^{out}(x, y)$, of a test model in one particular phase.

8. Application to accretion disc systems of TT Hya type

As another and more realistic example or test of the code, we have chosen to calculate synthetic spectra of H_α with the geometry similar to the well-known Algol type binary TT Hya. The star exhibits the emission features which were ascribed to the disc (Plavec & Polidan 1976) surrounding the primary. This has been studied by Kulkarni & Abhyankar (1980), Plavec (1988), Peters (1989), Van Hamme & Wilson (1993), Albright & Richards (1996), Peters & Polidan (1998), Richards & Albright (1999). The secondary contributes little to the spectrum. If not stated otherwise, the calculations were performed with the relatively low xyz resolution of $76 \times 76 \times 76$ points and for the space region containing the primary and the disc. The primary was treated as a blackbody with the following

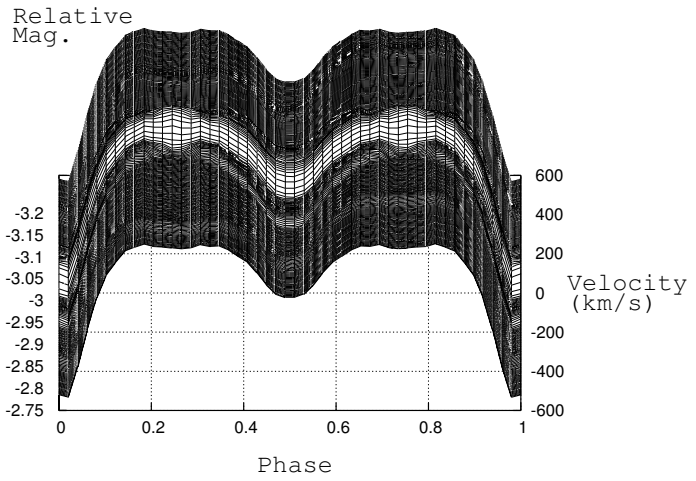

Figure 3. Overall light curve of the test model.

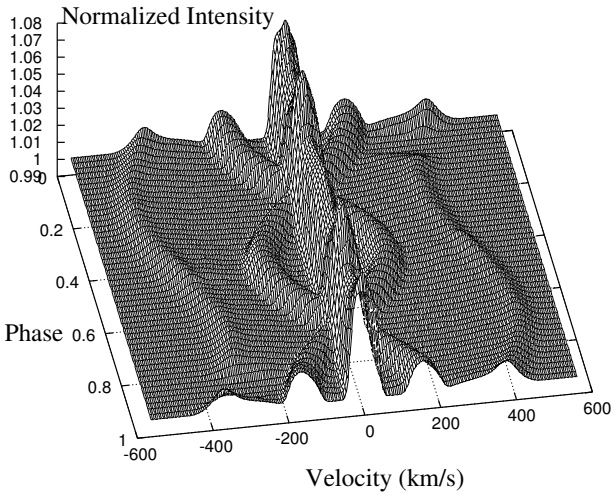

Figure 4. Trailed spectrogram of the test model.

parameters: effective temperature $T_{eff} = 9800K$, mass $M = 2.25M_{\odot}$, radius $R = 1.9R_{\odot}$ (Etzel 1988) and limb darkening $u = 0$. The disc was characterized by: inner radius $R_{in} = 2.5R_{\odot}$, outer radius $R_{out} = 10R_{\odot}$, angular halfwidth $\alpha = 15°$, electron number density $n_e = 3 \times 10^9 cm^{-3}$, density $\rho = 5 \times 10^{-15} g\, cm^{-3}$, temperature $T = 7000K$, microturbulence $v_{trb} = 0\, km\, s^{-1}$, and inclination $i = 84.4°$. The following pictures illustrate the effects of varying just one of many free parameters of the system.

Figures 5 and 6 display the effect of increasing the angular thickness of the disc from 10° to 80° (angular halfwidth from 5° to 40°). The overall emission increases as we increase the emitting space volume, and the central absorption decreases mainly for the higher angles. This occurs because the central depression is partly produced by the material projecting onto the star and there is more material in the Keplerian disc which does not project onto the stellar disc (surface) at higher angles, thereby filling the central absorption. Note also how the width of the central absorption changes. This is not true for small angles below 10° as it essentially causes the disc and its line profile to diminish.

Figures 7 and 8 display the effect of changing the outer radius of the disc from 6 to 14 $R_{\odot}$. The emission increases as the emission volume increases. This parameter has probably the strongest effect on the position of the emission peaks and width of the central depression. Peaks get closer for larger radius as more matter at lower Keplerian velocities is involved. The central absorption also varies slightly depending on the amount of the matter projected onto the stellar surface. This absorption first deepens and then for $R > 10R_{\odot}$ weakens as the thickness of the disc overcomes the radius of the primary. Blue and red wings of the line are not affected at all.

Figures 9 and 10 display the effect of increasing the inner radius of the disc from 2 to 8 $R_{\odot}$. Contrary to the outer radius, the inner radius has little effect on the emission from the beginning when it is a small fraction of the outer radius since it does not change the emission volume noticeably. The changes are mainly seen in the far wings of the profile as the higher Keplerian velocities are involved. Only when it approaches the outer radius, the overall emission starts to decline and the line weakens as the emission volume decreases, and the shape of the profile acquires the new U-type shape with a central hole. This shape indicates that the central depression is created by two different mechanisms (see below).

We also illustrate the profile shape if the disc were viewed from different inclination angles (Figure 11). Starting from edge-on, $i = 90°$, the two emission peaks have the lowest intensity as the 2D projection area of the disc is smallest (although the total emission volume is kept constant) and the disc may absorb more of its own light on its way to the observer. We also observe the largest separation of the emission peaks as we encounter the highest radial velocities and the deepest central depression as most of the disc which is cooler than the star projects onto the stellar surface. As the inclination decreases and we begin to see the disc pole-on the emission peaks increase and their separation and central depression vanish eventually merging into single peak emission for

$i = 0°$. One can also see that the central depression is caused by two different effects. The velocity field and geometry of the disc itself can produce the U or V type of the depression. Superposed on that is the absorption by the cool matter projected onto the hotter stellar surface which quickly diminish if viewed out of the disc plane.

Apart from state quantities and velocity field, every space point can be assigned a value of microturbulence. It is included in the calculation of thermal broadening as an additional thermal motion and can thus be used to model chaotic velocity fields on the scale smaller than the mean free path of a photon. It turns to be a useful free parameter as the mass transfer may not be a smooth process and the velocity field of the spiraling gas in the disc may well depart from the circular Keplerian orbits and be turbulent and these departures may easily exceed the sound velocity which is of the order of 10 $\mathrm{km\,s^{-1}}$. Figure 12 illustrates the effect of increasing the microturbulence in the disc from 0 to 60 $\mathrm{km\,s^{-1}}$. Note that the inner radius Keplerian disc velocity is about 400 $\mathrm{km\,s^{-1}}$. The emission peaks are gradually smoothed and are broader. The behavior of central absorption is more complicated and interesting. ¿From the beginning it gets narrower and deeper because of the desaturation effects of the microturbulence but then the smoothing effect prevails.

Figure 13 displays the effect of increasing the electron number density of the disc from 1×10^9 to $5 \times 10^9 cm^{-3}$. In this case, we assume that hydrogen is almost fully ionized, in which case the density is linearly proportional to the electron number density. This strongly enhances the emission peaks and slightly deepens the central absorption. This huge impact on the emission can be understood since the equivalent width in the optically thin case is proportional to the population of the particular level, which in turn is proportional to the total HI population. However, the ionization fraction of neutral hydrogen is proportional to the electron number density, and if the latter is also proportional to the density it follows that the total HI population increases with the square of the density or the electron number density assuming the hydrogen abundance and temperature are fixed ($n_{HI}/n_{HII} \approx n_{HI}/n_H \sim n_{HI}/\rho \sim n_e \sim \rho$). As a consequence, the equivalent width, EQW, should behave also like $\sim n_{HI} \sim \rho^2 \sim n_e^2$ which is seen in Figure 13.

Since the emission is so sensitive to the density we study the effect of different density profiles in Figure 14. Let the density and electron number density be inhomogeneous and have a power law dependence on the distance from the star, namely, $\rho \sim r^\eta$. This was achieved by varying the exponent $edendc \equiv \eta$ from -1.0 to +0.5 and by normalizing the synthetic spectrum to the same emission peak strength. It is apparent from the pictures that the line profiles for lower exponents have broader wings while those for higher exponents have narrower central depression. It can easily be explained as the lower exponents emphasize the matter close to the star with higher Keplerian velocity while the opposite is true for the higher exponents. It is interesting that the position of the peaks does not vary much.

Figures 15 and 16 display the effect of varying the temperature of the disc over an interval from 5000-10000K. The emission is strongest at about 7000K and declines towards higher temperatures as the fraction of neutral hydrogen declines due to ionization. The emission also declines towards cooler temperatures as it decreases the population of the lower level from which the H_α originates. At the same time, the temperature of the disc has a strong effect on the depth of the central absorption which grows towards the cooler temperatures within the range $10000 > T > 6000K$ because the source function along the line of sight hitting the stellar surface steps down from the stellar surface to disc and towards the observer. For cooler temperatures, the line-to-continuum emissivity decreases (the continuum is provided by the star mainly) and the line disappears from the spectrum forcing the central depression to merge with continuum as well. The central absorption seems strongest at about 6000K.

All of the previous calculations decribed above were carried out assuming the primary as a blackbody, i.e. having a smooth continuous spectrum. It was very convenient to grasp the effect of one parameter on the spectrum at a time. In reality, the primary star (as well as the secondary) has its own spectrum, where the H_α is not negligible and in fact dominates the optical spectrum of Algol-type binaries. That is why the tiny effects of such a small disc are usually difficult to uncover unless the stellar spectrum is removed. Difference profiles are calculated by subtracting the spectra of the stars from the observed spectrum to enhance the contribution of the unknown sources (Richards 1993; Richards & Albright 1999). This suggests that if the normalized continuum (value =1) is subtracted from our calculations above they could be interpreted as difference profiles which describe the contribution of the disc. To verify the extent to which such an approximation is good we calculated a synthetic spectrum of the primary (no black body anymore) with the code SYNSPEC (Hubeny et al. 1994, Krtička 1998). We assumed zero rotational velocity to study the most extrem case of H_α line. This spectrum was then assigned to the primary and a more complex spectrum of the disc and primary was calculated using SHELLSPEC. This combined spectrum is displayed in Figure 17. Consequently, we subtracted that synthetic spectrum of the primary (not the value=1) from this combined spectrum and were left with the difference profile which is compared with the difference profile obtained from the earlier calculations (primary as a blackbody) by subtracting an intensity of 1 from the data. The result is displayed in Figure 18 in which the profiles look similar except that the blackbody approximation of the star overestimates the depth of the central depression. So, under certain circumstances the blackbody primary may be a reasonable approximation in calculating the difference profiles unless the depth of the central depression is important, in which case the exact treatment of the primary with its own precalculated spectrum is highly recommended.

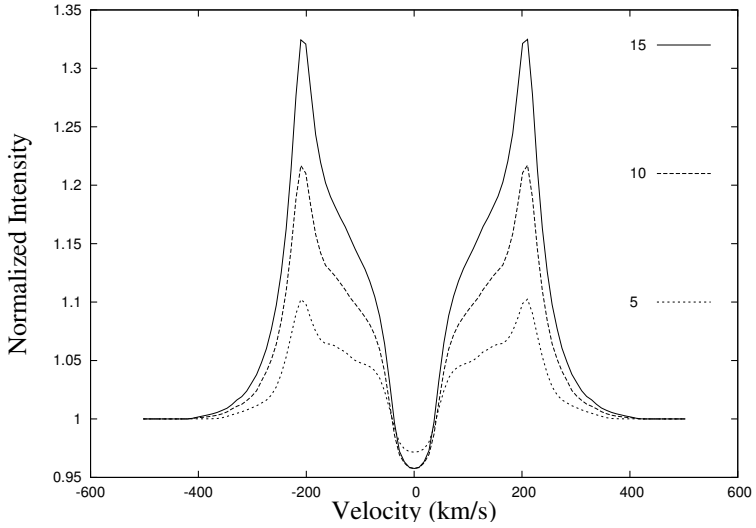

Figure 5. Effect of varying alpha (angular half-width of the disc) from 5 to 15 degrees.

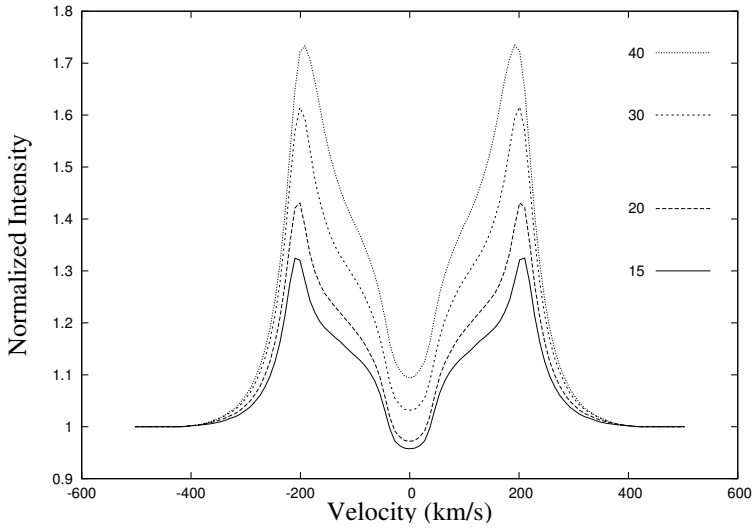

Figure 6. Effect of varying angular half-width of the disc from 15 to 40 degrees.

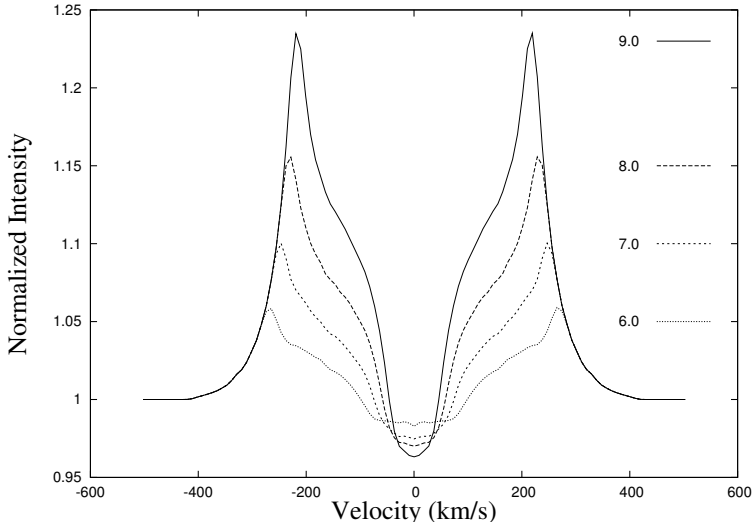

Figure 7. Effect of varying the outer radius of the disc from 6 to 9 $R_\odot$.

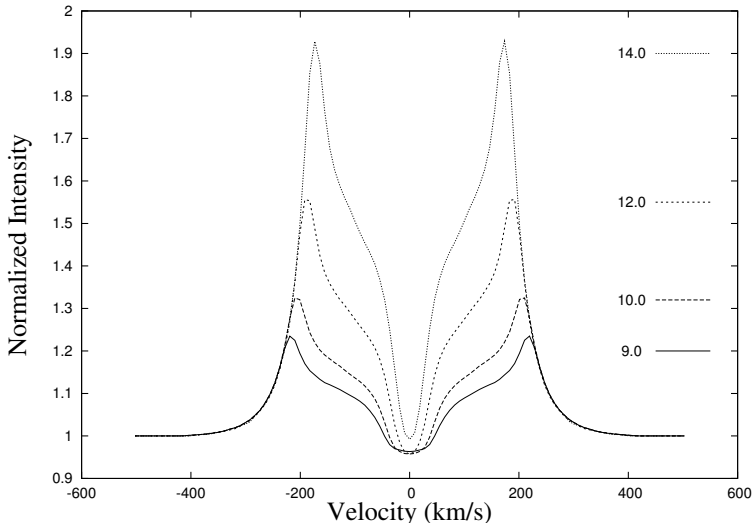

Figure 8. Effect of varying the outer radius of the disc from 9 to 14 $R_\odot$.

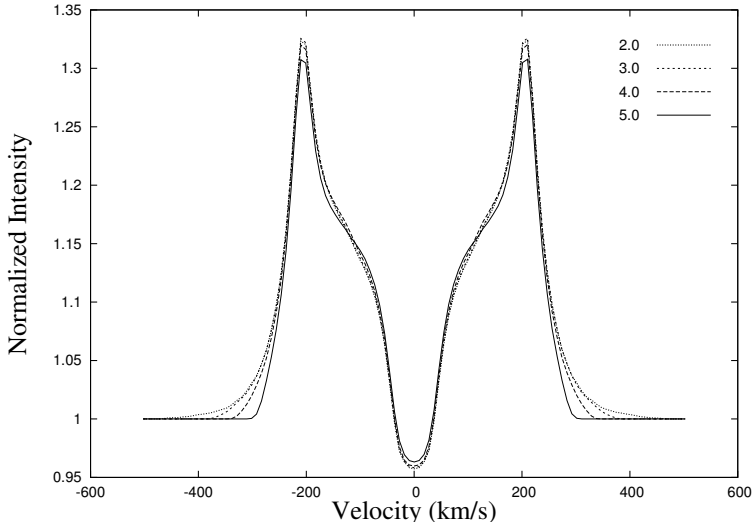

Figure 9. Effect of varying the inner radius of the disc from 2 to 5 $R_\odot$.

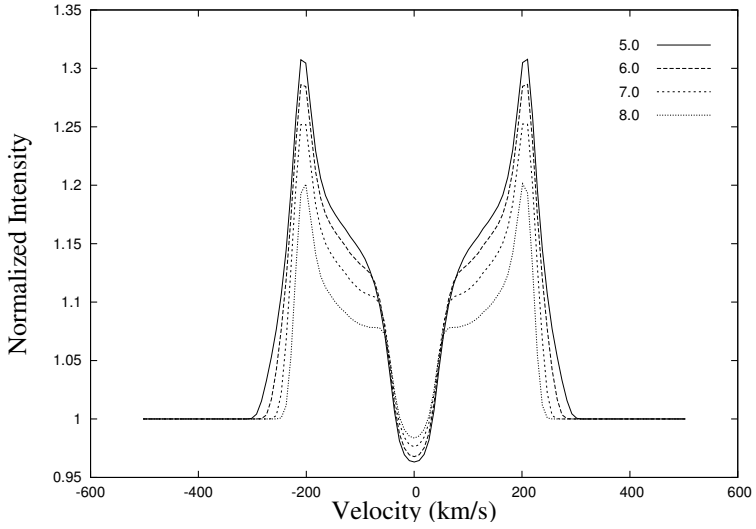

Figure 10. Effect of varying the inner radius of the disc from 5 to 8 $R_\odot$.

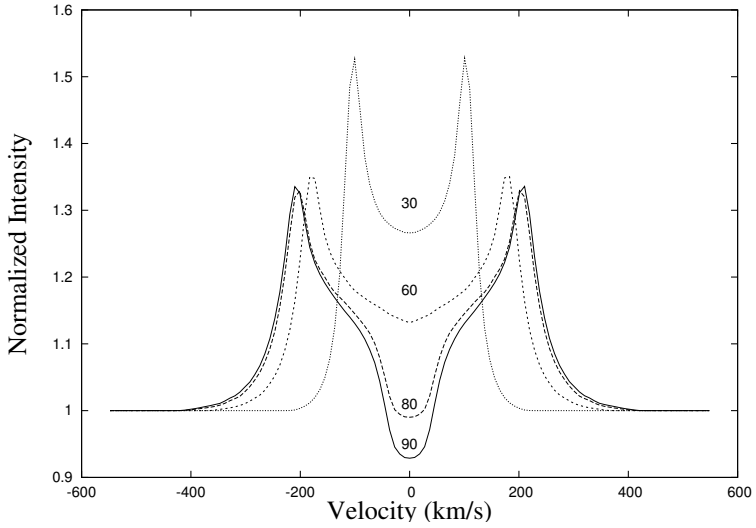

Figure 11. Effect of changing the inclination of the disc from 90° to 30°.

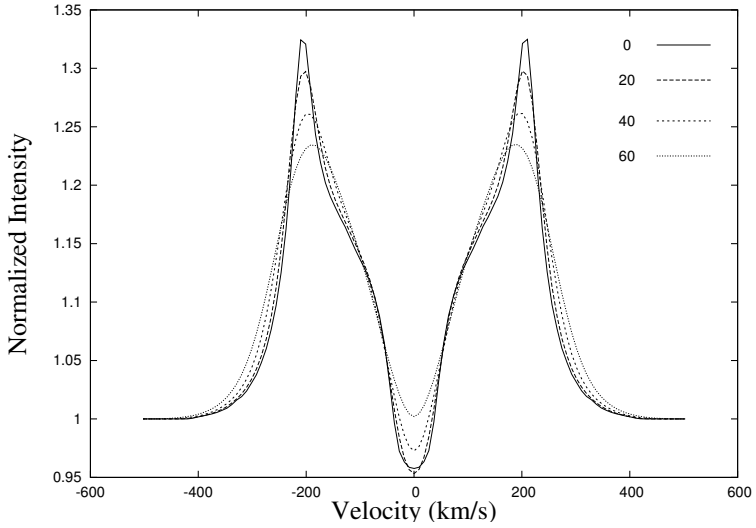

Figure 12. Effect of increasing the microturbulence in the disc from 0 to 60 $\mathrm{km\,s^{-1}}$.

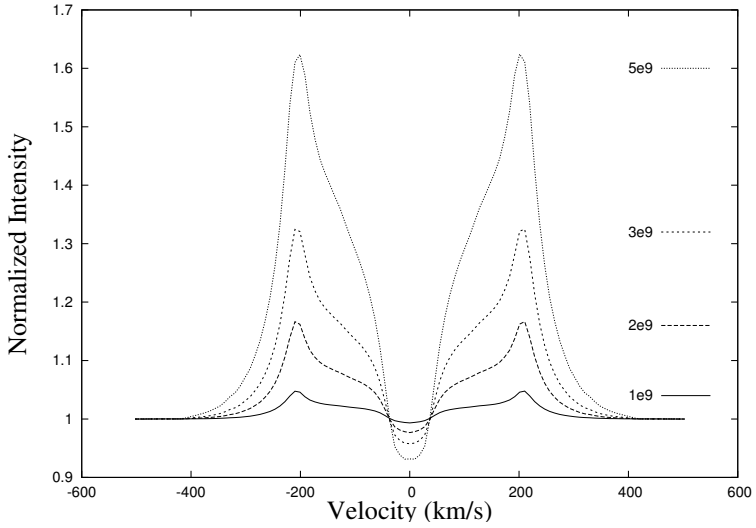

Figure 13. Effect of varying the density and the electron number density of the disc. n_e varies from 1×10^9 to $5 \times 10^9 cm^{-3}, \rho \sim n_e$.

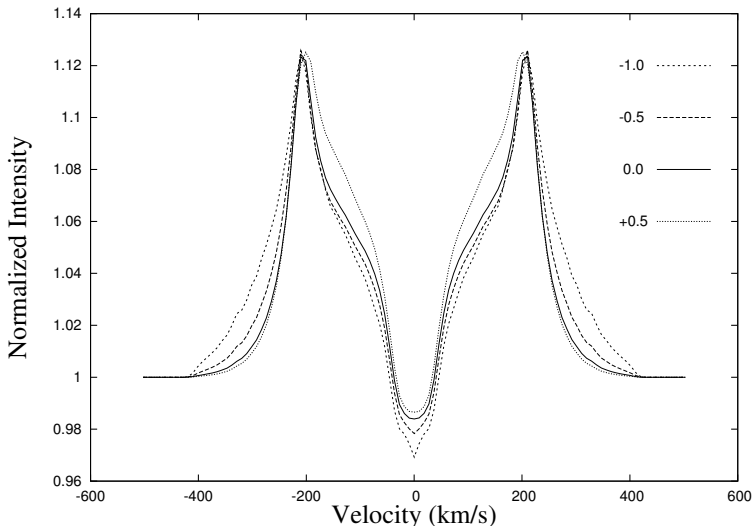

Figure 14. Effect of varying the exponent η of the power law behavior of the densities $\rho \sim r^\eta$ in the disc, $\eta = -1.0, -0.5, 0., +0.5$.

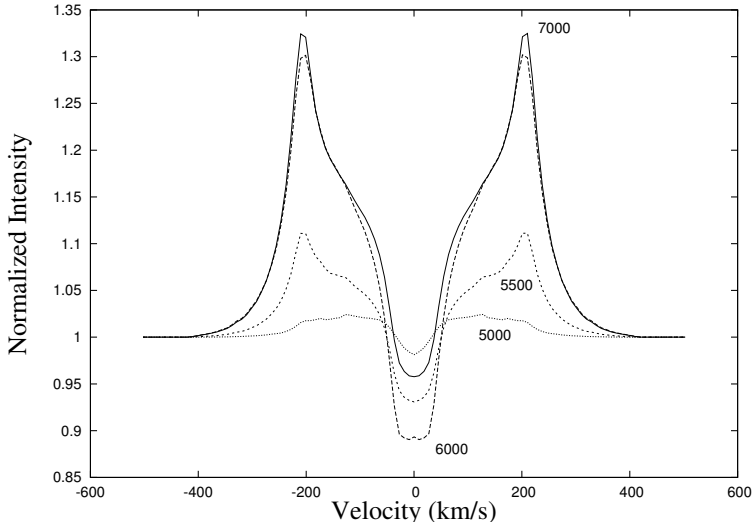

Figure 15. Effect of varying temperature of the disc from 5000K to 7000K.

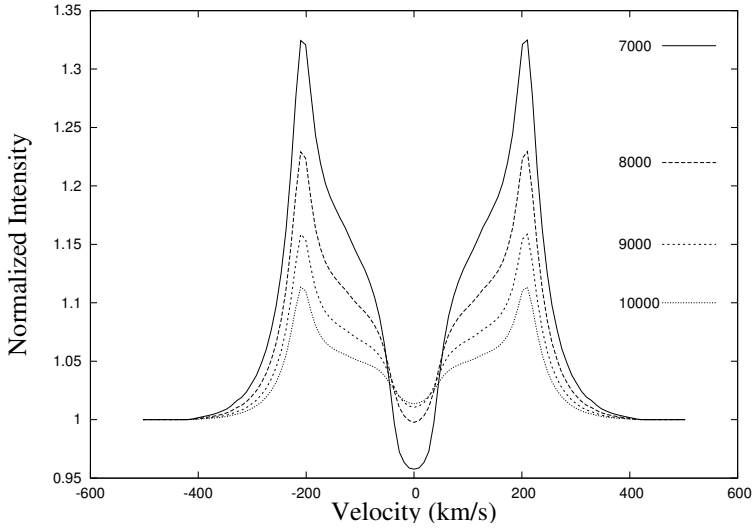

Figure 16. Effect of varying temperature of the disc from 7000K to 10000K.

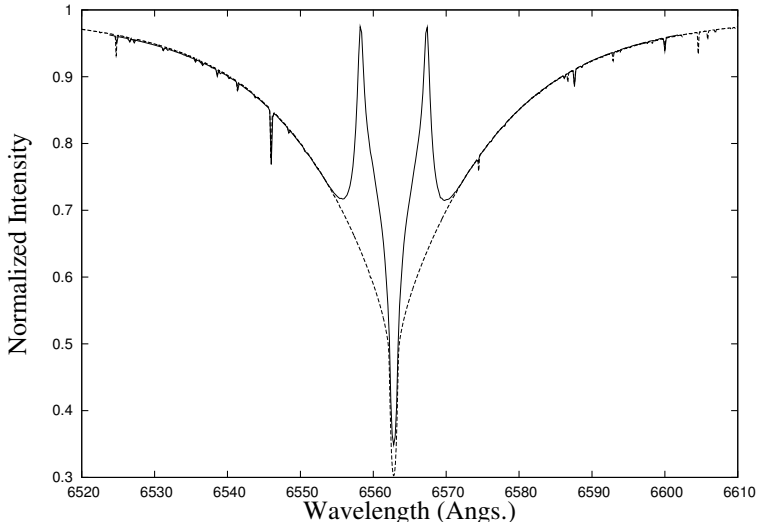

Figure 17. Synthetic spectrum of the primary (dashed line), composite synthetic spectrum of the primary with disc (solid line).

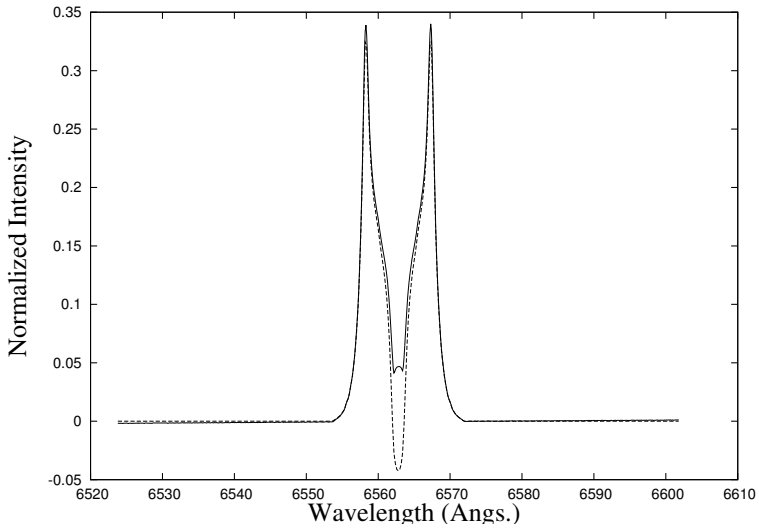

Figure 18. Difference profiles calculated when primary has its own intrinsic spectrum (solid line) or when primary was treated as a blackbody (dashed line).

Acknowledgements. We would like to thank Drs. J. Kubát, A. Skopal and an anonymous referee for their comments and suggestions. JB gratefully acknowledges grant support from Penn State University and thanks Drs. K. Getman, M. Tsujimoto, and the department computer staff for their assistance with computer related problems. This research was supported by the NSF-NATO fellowship (NSF DGE-0312144) and partly by the VEGA grant No. 3014 from the Slovak Academy of Sciences and the Science and Technology Assistance agency under the contract No. 51-000802. This study made use of the Vienna Atomic Line Data Base (VALD) services.

References

Albright, G.E., Richards, M.T.: 1996, *Astrophys. J.* **459**, L99
Bradstreet, D.H., Steelman, D.P.: 2002, *Bull. Am. Astron. Soc.* **34**, 1224
Budaj, J., Dworetsky, M.M.: 2002, *Mon. Not. R. Astron. Soc.* **337**, 1340
Budaj, J., Dworetsky, M.M., Smalley, B.: 2002, *Comm. Univ. London Obs.* **82** URL=http://www.ulo.ucl.ac.uk/ulo_comms/82/index.html
Cherepashchuk, A.M., Eaton, J.A., Khaliullin, K.F.: 1984, *Astrophys. J.* **281**, 774
Djurasevic, G.: 1992, *Astrophys. Space Sci.* **197**, 17
Drechsel, H., Haas, S., Lorenz, R., Mayer, P.: 1994, *Astron. Astrophys.* **284**, 853
Etzel, P.B.: 1988, *Astron. J.* **95**, 1204
Grevesse, N., Sauval, A.J.: 1998, *Space Sci. Rev.* **85**, 161
Gray, D.F.: 1976, *Observation and analysis of stellar photospheres*, A Wiley-Interscience publ., New York
Hadrava, P.: 1997, *Astron. Astrophys., Suppl. Ser.* **122**, 581
Hill, G.: 1979, *Publ. Dom. Ap. Obs. Victoria* **15**, 297
Hilditch, R.W.: 2001, *An introduction to close binary stars*, Cambridge Univ. Press, Cambridge
Horne, K., Marsh, T.R.: 1986, *Mon. Not. R. Astron. Soc.* **218**, 761
Hubeny, I.: 1988, *Comput. Phys. Comm.* **52**, 103
Hubeny, I., Lanz, T.: 1992, *Astron. Astrophys.* **262**, 501
Hubeny, I., Lanz, T.: 1995, *Astrophys. J.* **439**, 875
Hubeny, I., Lanz, T., Jeffery, C.S.: 1994, in Newsletter on Analysis of Astronomical spectra No.20, ed. C.S. Jeffery (CCP7; St. Andrews: St. Andrews Univ.), 30
Kopal, Z.: 1959, *Close Binary Systems*, Chapman & Hall Ltd., London
Krtička, J.: 1998, in *Proc. 20th Stellar Conf.*, eds.: J. Dušek and M. Zejda, Nicholas Copernicus Observatory and Planetarium, Brno, 73
Krtička, J., Kubát, J.: 2002, *Astron. Astrophys.* **388**, 531
Kubát, J.: 2001, *Astron. Astrophys.* **366**, 210
Kulkarni, A.G., Abhyankar, K.D.: 1980, *Astrophys. Space Sci.* **67**, 205
Kupka, F., Piskunov, N.E., Ryabchikova, T.A., Stempels, H.C., Weiss, W.W.: 1999, *Astron. Astrophys., Suppl. Ser.* **138**, 119
Kurucz, R.L.: 1970, SAO Special Report 309
Kurucz, R.L.: 1993a, SYNTHE spectrum synthesis programs and line data (Kurucz CD-ROM 18)
Kurucz, R.L.: 1993b, ATLAS9 Stellar Atmosphere Programs and 2km/s grid (Kurucz CD-ROM 13)
la Dous, C.: 1989, *Astron. Astrophys.* **211**, 131

Long, K.S., Knigge, C.: 2002, *Astrophys. J.* **579**, 725
Lucy, L.B.: 1968, *Astrophys. J.* **153**, 877
Mihalas, D.: 1978, *Stellar Atmospheres*, W.H. Freeman and company, San Francisco
Mochnacki, S.W., Doughty, N.A.: 1972, *Mon. Not. R. Astron. Soc.* **156**, 51
Orosz, J.A., Wade, R.A.: 2003, *Astrophys. J.* **593**, 1032
Peters, G.J.: 1989, *Space Sci. Rev.* **50**, 9
Peters, G.J., Polidan, R.S.: 1998, *Astrophys. J.* **500**, L17
Plavec, M., Kratochvil, P.: 1964, *Bull. Astron. Inst. Czechosl.* **15**, 165
Plavec, M.J., Polidan, R.S.: 1976, in *IAU Symp. 73, Structure and Evolution of Close Binary Systems*, eds.: P. Eggleton , S. Mitton and J. Whelan, Reidel, Dordrecht, 289
Plavec, M.J.: 1988, *Astron. J.* **96**, 755
Press, W.H., Flannery, B.P., Teukolsky, S.A., Vetterling, W.T.: 1986, *Numerical Recipes*, Cambridge Univ. Press, Cambridge
Pribulla, T.: 2004, in *Spectroscopically and Spatially Resolving the Components of Close Binary Stars*, ed.: R. Hilditch et al., ASP Conf. series., in press, ,
Pringle, J.E.: 1981, *Ann. Rev. Astron. Astrophys.* **19**, 137
Proga, D., Kallman, T.R., Drew, J.E., Hartley, L.E.: 2002, *Astrophys. J.* **572**, 382
Richards, M.T.: 1993, *Astrophys. J., Suppl. Ser.* **86**, 255
Richards, M.T., Albright, G.E.: 1999, *Astrophys. J., Suppl. Ser.* **123**, 537
Richards, M.T., Ratliff, M.A.: 1998, *Astrophys. J.* **493**, 326
Rucinski, S.W.: 1973, *Acta Astron.* **23**, 79
Rybicki, G.B., Hummer, D.G.: 1983, *Astrophys. J.* **274**, 380
Smith, K.C.: 1992, PhD thesis, University of London
Smith, K.C., Dworetsky, M.M.: 1988, in *Elemental Abundance Analyses*, eds.: S.J. Adelman and T. Lanz, Institut d'Astronomie de l'Univ. de Lausanne, Switzerland, 32
Van Hamme, W., Wilson, R.E.: 1993, *Mon. Not. R. Astron. Soc.* **262**, 220
Vinkó, J., Hegedüs, T., Hendry, D.: 1996, *Mon. Not. R. Astron. Soc.* **280**, 489
Wade, R.A., Hubeny, I.: 1998, *Astrophys. J.* **509**, 350
Wilson, R.E., Devinney, E.J.: 1971, *Astrophys. J.* **166**, 605
Zhang, E.-H., Robinson, E.L., Nather, R.E.: 1986, *Astrophys. J.* **305**, 740